Mechanisms of orthopyroxene dissolution in silica-undersaturated melts at 1 atmosphere and implications for the origin of silica-rich glass in mantle xenoliths

Article *in* Contributions to Mineralogy and Petrology · September 1998

DOI: 10.1007/s004100050429

CITATIONS
85

READS
109

4 authors, including:

Cliff S. J. Shaw
University of New Brunswick
70 PUBLICATIONS **1,384** CITATIONS
SEE PROFILE

Yves Thibault
Natural Resources Canada
49 PUBLICATIONS **1,218** CITATIONS
SEE PROFILE

Contrib Mineral Petrol (1998) 132: 354–370

Cliff S.J. Shaw · Yves Thibault · Alan D. Edgar
Felicity E. Lloyd

Mechanisms of orthopyroxene dissolution in silica-undersaturated melts at 1 atmosphere and implications for the origin of silica-rich glass in mantle xenoliths

Received: 30 August 1996 / Accepted: 15 April 1998

Abstract Experiments dissolving orthopyroxene (En_{93}) in a variety of Si-undersaturated alkaline melts at 1 atmosphere and variable f_{O_2} demonstrate that orthopyroxene dissolves to form olivine, Si-rich melt and clinopyroxene. These phases form a texturally and chemically distinct boundary layer around the partly dissolved orthopyroxene crystals. The occurrence of clinopyroxene in the boundary layer is due to inward diffusion of Ca from the solvent melt to the boundary layer causing clinopyroxene saturation. Compositional profiles through the solvent and the boundary layer for a number of experiments demonstrate rapid diffusion of cations across the boundary layer – solvent interface. SiO_2 diffuses outward from the boundary layer whereas CaO and Al_2O_3 diffuse toward the Si-enriched boundary layer melt. The rate of Al diffusion is slower under reducing conditions compared to the rates in experiments performed in air. Concentrations of FeO and MgO in the boundary layer and solvent are approximately equal indicating rapid diffusion and attainment of equilibrium despite ongoing crystallisation of clinopyroxene within the boundary layer. The behaviour of Na_2O and K_2O is strongly affected by f_{O_2}. Under reducing conditions Na_2O and K_2O concentrations are approximately equal in the boundary layer and solvent indicating normal diffusion down the concentration gradient and attainment of equilibrium. Under oxidising conditions, K_2O and to a lesser extent Na_2O, have compositional profiles indicative of uphill diffusion likely due to their preference for more polymerised Si- and Al-rich melts. Under reduced conditions Al-enrichment in the boundary layer melt is not as extreme and uphill diffusion did not occur. The composition of the solvent melt after the experiments indicates that it was contaminated by the boundary layer by convective mixing due to the onset of hydrodynamic instabilities brought on by density and viscosity contrasts between the two melts. Despite using a wide variety of solvent melt compositions we find that the boundary layer melts converge toward a common composition at high SiO_2 contents. The composition of glass generated by orthopyroxene dissolution at 1 atmosphere is similar in many respects to Si-rich glass found in many orthopyroxene-rich mantle xenoliths that have been attributed to high pressure in situ processes including mantle metasomatism. The results of this study suggest that at least some Si-rich melts are likely to have formed by dissolution of xenolith orthopyroxene at low pressure possibly by their Si-undersaturated host magmas.

C.S.J. Shaw ✉
Bayerisches Geoinstitut, Universität Bayreuth,
95440 Bayreuth, Germany
E-mail: cliff.shaw@uni-bayreuth.de

Y. Thibault
Department of Earth Sciences, University of Western Ontario,
London, Ontario N6A 5B7, Canada

A.D. Edgar†
Department of Earth Sciences, University of Western Ontario,
London, Ontario N6A 5B7, Canada

F.E. Lloyd
Department of Geology, University of Bristol, Wills Memorial
Building, Queens Road, Bristol BS8 1RJ, England

Editorial responsibility: K. Hodges

Introduction

Mantle metasomatism is important to our understanding of the genesis of many mafic, alkaline magmas. Despite recognition of metasomatism as an important process, there is still considerable controversy over the nature of the agent and the process by which it takes place (Bailey 1987; Menzies et al. 1987; Edgar 1997). In recent years several workers have suggested that Si-enriched glass inclusions in mantle xenoliths may represent the quenched remains of metasomatic melts (Gamble and Kyle 1987; Edgar et al. 1989; Schiano and Clocchiatti 1994; Szabo et al. 1996; O'Connor et al. 1996). However, the origin of glass inclusions in mantle xenoliths remains controversial (see Hauri et al. 1993;

Ionov et al. 1994; Wilshire and McGuire 1996) and at least nine hypotheses have been put forward to explain their formation (Table 1). Examination of glass compositions from orthopyroxene-bearing and orthopyroxene-free xenoliths shows a general division into SiO_2-poor and SiO_2-rich varieties respectively (Yaxley et al. 1997 and Fig. 1) which suggests that orthopyroxene may play a role in the genesis of Si-rich glass. In addition, there is clear evidence that reaction between orthopyroxene and silica-undersaturated melt produced Si-rich glass in many mantle xenoliths (Tracy 1980; Francis 1987; Edgar et al. 1989; Chazot et al. 1996; Yaxley et al. 1997; Shaw and Edgar 1997). However, there are few constraints on the mechanism and controls of reaction particularly with reference to pressure, f_{O_2} and changing solvent melt composition.

We have examined the composition of melts produced by dissolution of orthopyroxene in three different alkali-rich Si-undersaturated melts. The purpose of this work is:

(1) To determine if orthopyroxene dissolution at 1 atmosphere can produce Si-, Al-, alkali-rich glass and to examine the implications of an orthopyroxene – Si-undersaturated melt reaction on the origin of mantle xenolith glasses.

(2) To define the mechanism by which dissolution occurs and the effects of changing intensive variables such as f_{O_2}.

(3) To test the suggestion of Francis (1987) that the composition of silicate melts buffered by lherzolite will be broadly andesitic at 1 bar. If this assertion is correct, the melts produced by reaction of the three solvents should give a broadly similar composition.

(4) To resolve chemical and textural criteria that can be used to recognise the effects of low pressure orthopyroxene dissolution in igneous rocks.

Experimental

We did the experiments at 1 bar rather than mantle pressures since the presence of olivine in silica-rich melts around dissolved orthopyroxene (Zinngrebe and Foley 1995; Tracy 1980; Shaw and Edgar; 1997) suggests that the reaction involves the incongruent breakdown of orthopyroxene, that occurs at pressures less than ~5 kb (Boyd et al. 1964). Experiments on orthopyroxene dissolution rates in moderately alkali-rich basalt (Brearly and Scarfe 1986) noted that at 5 kb orthopyroxene broke down to olivine + melt. However, at 12 kb olivine was not present.

Starting materials

The orthopyroxene used in all the experiments is an aluminous enstatite from Andhra-Pradish, India (Table 2). Several pieces of this material were examined both optically and by electron microprobe to check for homogeneity. The crystals were cleaned in dilute HCl and then in an ultrasonic bath for 30 min and were stored in a drying oven at 150 °C until required.

To examine the effects of changing the SiO_2, Al_2O_3, CaO and alkali contents of the solvent melt on the products of dissolution we chose three melt compositions (Table 2):

(1) An evolved basanite derived by approximately 90% partial melting of a primitive basanite from Gees, West Eifel, Germany.
(2) A synthetic mugearite.
(3) A synthetic phonotephrite.

The synthetic glasses were prepared by multiple fusion of carefully weighed and dried reagent grade oxides and carbonates at

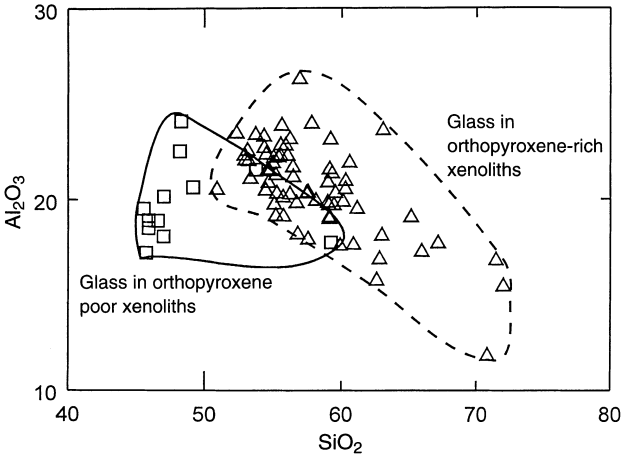

Fig. 1 Comparison of xenolith glass compositions from orthopyroxene-poor and orthopyroxene-rich xenoliths. (Data sources: O'Connor et al. 1996; Schiano and Clocchiatti 1994; Schiano et al. 1994; Dautria et al. 1992; Hansteen et al. 1991; Jones et al. 1983; Francis 1976a, b; Ionov et al. 1994; Gamble and Kyle 1987; Ionov et al. 1993; Draper 1992; Edgar et al. 1989; Yaxley et al. 1997)

Table 1 Hypotheses for the origin of glass inclusions in mantle xenoliths

Origin of Glass	References
Residual liquids in incompletely crystallised rocks	Hermes and Cornell (1981), Hansteen et al. (1991)
Quenched infiltrated host magma	Garcia and Presti (1987)
Formed due to decompression and heating on entrainment of the xenoliths	Frey and Green (1974), Padovani and Carter (1977)
Partial melting formed on heating by intrusions in the source region	Carpenter (1996)
Partial melting due to general heating of the source region	Kuo and Essene (1986)
Glasses represent melts which infiltrated the mantle prior to xenolith entrainment	Gamble and Kyle (1987), Edgar et al. (1989), O'Connor et al. (1996), Schiano and Clocchiatti (1994)
Melting induced by the influx of metasomatic fluids	Ionov et al. (1994)
Fractionation of phlogopite and amphibole from an infiltrated Si-undersaturated melt	Szabo et al. (1996)
Reaction between host magma and xenolith minerals during ascent	Shaw and Edgar (1997)

Table 2 Composition of starting materials

Solvent f_{O_2}	Opx[a]	Solvents			
		UWO 1 Basanite Air	Q 2 Mugearite QFM	DPX 3a Phonotephrite QFM	DPX 3b Air
Wt%					
SiO_2	57.10	45.49	54.01	48.12	48.87
TiO_2	0.02	3.06	3.46	4.39	3.10
Al_2O_3	2.11	15.98	11.47	9.46	9.64
FeO	5.02	10.17	7.33	7.39	8.32
MnO	0.13	0.16	0.16	0.15	0.16
MgO	34.52	5.06	6.77	8.78	8.43
CaO	0.81	11.85	8.36	12.25	12.14
Na_2O	0.15	2.53	5.56	6.25	6.11
K_2O	0.02	3.90	2.24	2.46	2.45
P_2O_5	ND	0.67	0.63	0.76	0.77
Total	100.28	98.87	99.99	100.01	99.99
FeO[b]		1.93	5.93	5.72	0.95
Fe_2O_3[b]		9.18	1.55	1.84	8.12
K_2O/Na_2O		1.54	0.40	0.39	0.40
Liquidus Temperature[c]		1235	1200	1180	1180
Density (g/cm^3)[d]		2.971	2.813	2.907	2.915

[a] Includes 0.29% Cr_2O_3 and 0.11% NiO
[b] Fe_2O_3 and FeO calculated using the melts calculator (Ghiorso and Sack 1995)
[c] From Shaw (unpublished data)
[d] Calculated using data from Bottinga and Weill (1970), Bottinga et al. (1982)

1350 °C. The natural and synthetic solvent samples were crushed to a grain size of 100 mesh in an agate mortar and pestle and stored in a drying oven until required.

Experimental techniques

Basanite solvent

Two orthopyroxene crystals about 3 mm in size were placed in Pt foil bags with approximately 1 g of powdered basanite. These bags were suspended in the hot spot of a vertical quench furnace at 1220 °C for variable times. Oxygen fugacity was not buffered. Temperature was monitored using a Pt-Rh_{10}-Pt_{90} thermocouple accurate to within ±10 °C. No Fe was lost to the Pt foil during the experiments due to the oxidising conditions imposed. At the end of each experiment the charges were quenched in water. Details of the experimental conditions and durations are given in Table 3.

Mugearite and phonotephrite solvents

In these experiments, an orthopyroxene crystal approximately 4 mm in size was placed in a Fe-soaked Pt wire basket and was covered with approximately 600 mg of powdered solvent held together by polyvinyl alcohol binder. Temperature was monitored using a Pt-Rh_{10}-Pt_{90} thermocouple accurate to ±10 °C.

Experiments using the mugearite solvent were done at 1190 °C under controlled f_{O_2} conditions (QFM) in a CO-CO_2 gas mixing furnace. Oxygen fugacity was monitored using CSIRO f_{O_2} sensors. The experiments with the phonotephrite solvent were carried out at 1190 °C but were split into two groups. The first group were done at f_{O_2} = QFM buffer and the second group were done in air. To assess alkali loss during the experiments each dissolution experiment was accompanied by a solvent only charge. Analysis of these charges indicates that Na loss is small (less than 4% relative) due to the low flow rate of the CO-CO_2 gas mixtures. Fe loss to the Fe-soaked Pt in the f_{O_2} buffered experiments is negligible based on analyses of the Pt wire before and after the experiments. All of the experiments were quenched by blowing a stream of compressed air over the melt beads. Details of the experimental conditions and durations are given in Table 3.

Phase relations of the solvents

The liquidus temperatures, determined in a separate study (Shaw unpublished data), and calculated density (Bottinga and Weill 1970; Bottinga et al. 1982) of the three solvents are given in Table 2. The basanite and mugearite have clinopyroxene as their liquidus phase (Table 4) and in a few samples there is minor quench olivine. The phonotephrite solvent was above its liquidus temperature in all of the experiments. The SiO_2 and Al_2O_3 content of the clinopyroxene varies with solvent composition. Those from the basanite are Si- and Na-poor and Al- and Fe-rich relative to those from the Si- Mg- and Na-enriched and Al-poor mugearite solvent (Table 4).

In terms of melt composition and mineral composition there are minor differences in the composition of the buffered and unbuffered phonotephrite melts (Table 2). The unbuffered melts have marginally higher total FeO compared with the QFM buffered glass. Calculated Fe_2O_3 and FeO (using MELTS software, Ghiorso and Sack 1995) show that FeO/Fe_2O_3 varies from 0.11 to 0.21 for samples equilibrated in air to 3.1 to 5.8 for those samples equilibrated at the QFM buffer.

Analytical methods

Samples prepared with the basanite solvent were analysed using a JEOL-8600 electron microprobe at the University of Western Ontario. The mugearite and phonotephrite experiments were analysed with a Cameca SX-50 electron microprobe at the Bayerisches Geoinstitut.

The minerals in the basanite experiments were analysed with a focused electron beam and an accelerating voltage of 15 kV, a

Table 3 Run conditions and results

Run #	Solvent[a]	Duration (mins)	Temperature °C	f_{O_2}	Remarks
UWO-1	1	6	1220	Air	Glass only, opx not added
UWO-2	1	30	1220	Air	Glass + olivine + clinopyroxene + Cr-spinel
UWO-7	1	60	1220	Air	Glass + olivine + clinopyroxene + Cr-spinel
UWO-4	1	120	1220	Air	Glass + olivine + clinopyroxene + Cr-spinel
UWO-5	1	180	1220	Air	Glass + olivine + clinopyroxene + Cr-spinel
UWO-9	1	720	1220	Air	Glass + olivine + clinopyroxene + Cr-spinel
UWO-8	1	1260	1220	Air	Glass + olivine + clinopyroxene + Cr-spinel
UW0-10	1	1440	1220	Air	Glass + olivine + clinopyroxene + Cr-spinel
UWO-12	1	2880	1220	Air	Glass + olivine + clinopyroxene + Cr-spinel
Q-1	2	30	1190	QFM	Glass + olivine + clinopyroxene
Q-2	2	60	1190	QFM	Glass + olivine + clinopyroxene
Q-3	2	120	1190	QFM	Glass + olivine + clinopyroxene
Q-4	2	180	1190	QFM	Glass + olivine + clinopyroxene
Q-5	2	720	1190	QFM	Glass + olivine + clinopyroxene
Q-7	2	1440	1190	QFM	Glass + olivine + clinopyroxene
Q-8	2	2880	1190	QFM	Glass + olivine + clinopyroxene
Q-6	2	4320	1190	QFM	Glass + olivine + clinopyroxene
Q-9	2	4320	1190	QFM	Glass only, opx not added
DPX-14[b]	3	244	1190	Air	Glass + olivine + clinopyroxene + Cr-spinel
DPX-10	3	860	1190	Air	Glass + olivine + clinopyroxene + Cr-spinel
DPX-6	3	1440	1190	Air	Glass + olivine + clinopyroxene + Cr-spinel
DPX-2	3	2880	1190	Air	Glass + olivine + clinopyroxene + Cr-spinel
DPX-16	3	245	1190	QFM	Glass + olivine + clinopyroxene
DPX-12	3	860	1190	QFM	Glass + olivine + clinopyroxene
DPX-8	3	1440	1190	QFM	Glass + olivine + clinopyroxene
DPX-4	3	2880	1190	QFM	Glass + olivine + clinopyroxene

[a] Solvents: *1* evolved basanite, *2* synthetic mugearite, *3* synthetic phonotephrite
[b] Each DPX experiment was accompanied by a glass only charge

Table 4 Composition of clinopyroxene and quench olivine in the solvent melts

Solvent	Basanite				Mugearite			
Sample	UWO-1	UWO-1	UWO-1	UWO-1	Q9	Q9	Q9	Q9
f_{O_2}	Air	Air	Air	Air	FMQ	FMQ	FMQ	FMQ
Mineral	Olivine	Cpx	Cpx	Cpx	Olivine	Cpx	Cpx	Cpx
Wt%								
SiO_2	42.15	44.84	45.76	47.51	40.56	54.35	53.94	54.28
TiO_2	0.09	2.62	2.70	2.27	1.04	1.33	1.02	1.31
Al_2O_3	0.35	6.97	6.22	5.33	0.05	0.70	0.79	0.68
FeO	10.02	6.08	6.03	6.22	11.56	3.45	3.47	3.64
MnO	0.33	0.09	0.04	0.09	0.20	0.04	0.10	0.05
MgO	45.86	12.80	13.34	13.97	46.12	17.26	16.99	17.29
CaO	0.33	24.12	24.47	24.22	0.44	22.97	23.01	23.14
Na_2O	0.08	0.31	0.24	0.20	0.03	0.55	0.51	0.46
K_2O	0.01	0.20	0.03	0.00	0.02	0.01	0.01	0
Total	99.22	98.03	98.83	99.81	100.0	100.66	99.84	100.85
Mg#	0.90	0.81	0.81	0.82	0.89	0.91	0.91	0.90

probe current of 10 nA and counting times of 20 s for all elements except Na which was counted for 40 s. Glass was analysed using a defocused beam of 5 μm diameter to decrease loss of Na and K due to migration of these elements away from the beam (Nielsen and Sigurdson 1981). All data were processed using the Albee and Ray (1970) ZAF correction factors.

The mugearite and phonotephrite experiments were analysed with a 3 μm beam and an accelerating voltage of 15 kV and a current of 15 nA for both minerals and glass. Counting times were 20 s and the data were reduced using the PAP correction program. Tests using a beam size between 1 and 10 μm indicated that the 3 μm beam was the smallest that could be used while minimising alkali migration.

Dissolution basics

Dissolution rates may be controlled either by interface kinetics, i.e. the rate at which bonds are broken at the crystal – melt interface, or by the rate of removal of material from the dissolving crystal to the surrounding melt (Kuo and Kirkpatrick 1985). Most studies of mineral dissolution indicate that the rate controlling process is the

outward diffusion of material away from the dissolving crystal (Cooper and Kingery 1964; Kuo and Kirkpatrick 1985; Donaldson 1990). However, Thornber and Huebner (1985) present an alternative theory for olivine dissolution in which dissolution rate is controlled by interface kinetics. For orthopyroxene, the observation of constant dissolution rates with time (Brearly and Scarfe 1986; Edwards and Russell 1996) and the presence of a solute-rich film around the dissolving crystal is generally suggested to indicate that dissolution is controlled by diffusion away from the dissolving crystal (Donaldson 1990). This solute-rich film is referred to as a boundary layer and has been shown to be of essentially constant thickness regardless of experiment duration for various minerals (Donaldson 1990). As dissolution limited by chemical diffusion would result in a boundary layer whose thickness increased with time, most workers suggest that its thickness is kept constant due to compositional convection caused by density and viscosity contrasts between the solvent melt and the solute-rich boundary layer (Donaldson 1993; Macleod et al. 1996). Removal of boundary layer material from the dissolving crystal will result in contamination of the solvent.

Results

Textural and petrographic features

All of the experiments result in formation of a boundary layer of Si-rich glass, olivine and clinopyroxene around the orthopyroxene crystal (Fig. 2a–e). In experiments lasting less than 3 h, the boundary layer shows a distinct zonation (Fig. 2a): immediately adjacent to the orthopyroxene is a layer of glass, further out are sub- to euhedral crystals of olivine and on the outer margin of the layer are crystals of clinopyroxene, some of which contain melt inclusions. In the longer duration experiments this zonation is not present and olivine and clinopyroxene are intergrown (Fig. 2b–e). In the unbuffered experiments using basanite and phonotephrite there are small grains of Cr-rich oxide on the margin of the layer. These oxide grains are absent in the more reduced experiments suggesting that at the QFM buffer, oxide crystallisation is inhibited. Qualitative measurement of the reaction zone width shows that it is approximately constant in experiments of greater than 3 h duration, suggesting that either the reaction zone armours the orthopyroxene from further dissolution or the reaction zone is gradually removed as dissolution proceeds.

Point counting of the phases in the reaction zones indicates that the proportions of glass (45–50%), olivine (35–39%) and clinopyroxene (15–16%) are approximately constant and are independent of solvent composition, f_{O_2} or run duration for experiments with mugearite and phonotephrite solvents. In the experiments using a basanite solvent the proportion of clinopyroxene is much higher, up to 40%, at the expense of glass (20–30%). The proportion of olivine in all the experiments is much greater than that predicted from simple incongruent melting of orthopyroxene (Bowen and Anderson 1914).

The surface of the dissolving orthopyroxene is variably stepped to undulose and commonly the surface is pitted (Fig. 2a–e). These pits probably represent original heterogeneities on the mineral surface enhanced by dissolution. In experiments lasting more than 48 h, the solvent melt penetrated along the cleavage planes allowing dissolution to occur in the inner part of the orthopyroxene.

Comparison of the experimentally produced reaction zones (Fig. 2a–e) with those present on orthopyroxene from xenoliths (Fig. 2f) show close similarities. In the natural examples reaction zones consist of glass (10–20%), clinopyroxene (35–40%) and olivine (40–50%), in which the crystals have similar morphology and distribution to those in the experiments (Shaw and Edgar 1997; Shaw unpublished data).

Compositions

Boundary layer glass

Basanite solvent

Secondary glass around orthopyroxene dissolved by the basanite solvent shows distinct enrichment in SiO_2 and K_2O and minor enrichment in Na_2O coupled with depletion in FeO, CaO and minor depletion in Al_2O_3 compared with the solvent composition (Fig. 3, Table 5). It is worth noting here that in all the experiments the solvent composition has been changed relative to the original compositions. This is described further in a following section.

Seventeen analyses of boundary layer glass and solvent in UWO-9 show a distinct compositional discontinuity at the contact between the solvent and the boundary layer (Fig. 4). Solvent compositions do not vary over the length of the traverse. SiO_2 in the boundary layer glass increases towards the orthopyroxene to a maximum of 64 wt%. Al_2O_3, TiO_2, CaO and FeO decrease in the boundary layer glass with proximity to the orthopyroxene as expected since they are not abundant in orthopyroxene. Concentrations of MgO decrease slightly between the solvent and boundary layer and Na_2O has the same abundance in the boundary layer as in the solvent. However, K_2O is strongly enriched in the boundary layer relative to the solvent (Fig. 4).

Mugearite solvent

Glass in the boundary layer around orthopyroxene dissolved by the mugearite solvent shows similar trends to that noted above except that Al_2O_3 depletion is more pronounced and K_2O enrichment is less pronounced in the boundary layer glass (Table 5, Fig. 3).

A microprobe traverse across the solvent and boundary layer in sample Q-8 again shows a marked compositional discontinuity at the boundary layer solvent contact (Fig. 4). As for the experiments in basanite, the solvent compositions do not vary over the length of the

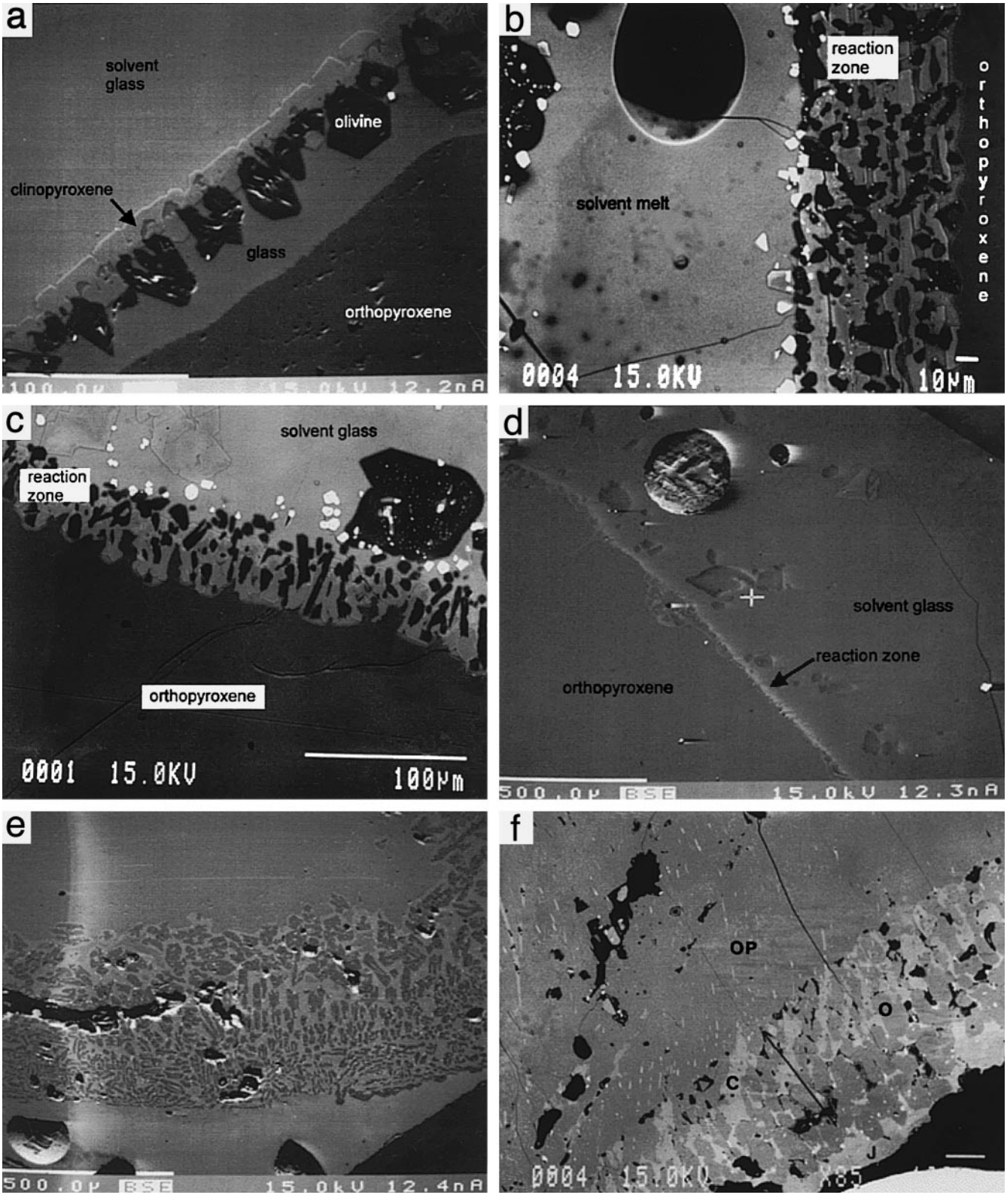

Fig. 2a–f Comparison of experimentally and naturally dissolved orthopyroxenes. **a** DPX-10, **b** UWO-9, **c** UWO-12, **d** Q3, **e** DPX 4, **f** Natural reaction zone in a lherzolitic xenolith from Gees, West Eifel, Germany. All photographs are backscattered electron images

traverse. Within the boundary layer SiO_2, FeO and to a lesser extent MgO all increase towards the orthopyroxene whereas Al_2O_3 and CaO decrease. The concentration of Na_2O and K_2O in the boundary layer and solvent are approximately equal. This contrasts with the un-

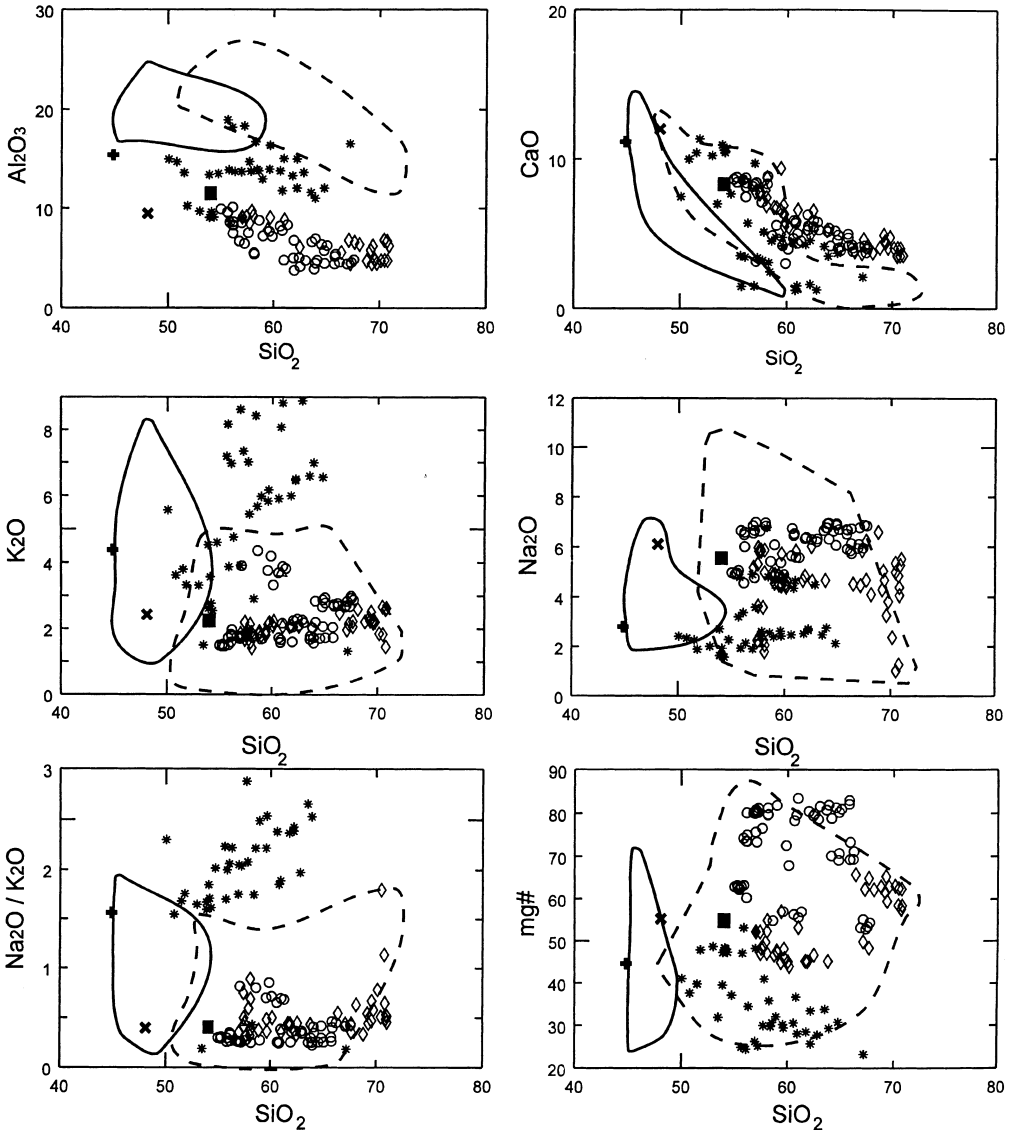

Fig. 3 Comparison of boundary layer glass compositions from the three series of experiments with Si-rich glass in mantle xenoliths. *Dashed field* glass in orthopyroxene-rich xenoliths, *solid field* glass in orthopyroxene-poor xenoliths (see Fig. 1 for data sources). *bold x* basanite solvent, *asterisk* basanite boundary layer glass, *filled square* mugearite solvent, *open diamonds* mugearite boundary layer glass, *bold upright cross* phonotephrite solvent, *open circles* phonotephrite boundary layer glass

buffered experiments in basanite solvent in which Al_2O_3 shows only a small decrease in the boundary layer relative to the solvent, K_2O shows distinctive enrichment in the boundary layer, and FeO and MgO are depleted.

These observations suggest that either changing solvent composition or f_{O_2} affect the behaviour of components diffusing into the boundary layer.

Phonotephrite solvent

The boundary layer glass formed by dissolution of orthopyroxene in phonotephrite melt under buffered and unbuffered conditions shows generally similar chemical trends to those of the boundary layer glass in the mugearite experiments (Fig. 3). However, detailed compositional traverses across the boundary layer and solvent in a buffered and unbuffered experiment (DPX 6 and 8) show distinct differences (Fig. 4, Table 5). In both cases SiO_2 is enriched towards the orthopyroxene. In the unbuffered experiment Al_2O_3 has approximately the same concentration in the boundary layer as in the solvent. However, in the QFM buffered experiment Al_2O_3 shows a strong depletion towards the orthopyroxene.

In both buffered and unbuffered experiments FeO decreases from the solvent towards the orthopyroxene although the overall concentrations are higher in the experiments in air relative to those under buffered f_{O_2}. MgO concentrations decrease towards the orthopyroxene in experiments done in air whereas in the buffered experiments MgO concentrations remain similar to that in the solvent or are slightly higher.

In both sets of experiment CaO decreases towards the orthopyroxene, whereas Na_2O shows distinctly different behaviour. In the unbuffered experiments Na_2O concentrations decrease slightly towards the orthopyroxene whereas in the buffered experiment Na_2O concentrations are higher than in the boundary layer glass. The experiment in air shows distinct K_2O enrichment in the boundary layer whereas in the boundary layer of the

Table 5 Glass compositions from dissolution experiments

	Basanite solvent													
Sample	*UWO*	UWO-2	UWO-7	UWO-7	UWO-4	UWO-4	UWO-5	UWO-5	UWO-9	UWO-9	UWO-8	UWO-10	UWO-12	UWO-12
Duration (min)		30	60	60	120	120	180	180	720	720	1260	1440	2880	2880
Type	*Solven t*	B.L.	B.L.	B.L.	B.L.	B.L.	B.L.	B.L.	B.L.	B.L.	B.L.	B.L.	B.L.	B.L.
SiO_2	*45.49*	50.58	50.58	57.70	50.53	52.68	51.08	56.97	57.82	59.58	56.07	59.65	64.78	63.92
TiO_2	*3.06*	2.68	1.63	0.98	2.35	1.92	1.91	1.49	1.56	1.42	1.24	0.96	0.99	0.46
Al_2O_3	*15.98*	14.02	13.76	14.67	10.90	9.73	10.25	9.03	13.69	13.91	18.19	16.36	12.01	11.02
FeO	*10.17*	6.63	4.08	4.97	8.45	8.63	7.41	7.13	5.28	5.44	3.34	3.47	4.79	5.86
MnO	*0.16*	0.14	0.17	0.03	0.12	0.18	0.12	0.05	0.07	0.12	0.11	0.15	0.09	0.05
MgO	*5.06*	6.79	11.38	3.36	10.25	9.91	8.44	8.43	5.56	3.51	2.24	2.92	3.44	3.46
CaO	*11.85*	10.63	4.84	3.22	11.63	11.69	11.37	9.72	5.13	4.76	3.44	4.18	3.69	3.50
Na_2O	*2.53*	2.10	2.65	2.43	1.49	1.45	1.89	1.91	2.62	2.63	3.38	2.43	2.13	2.76
K_2O	*3.90*	3.90	5.63	7.01	2.23	2.42	3.32	3.92	5.45	5.84	6.97	6.17	6.55	6.99
P_2O_5	*0.67*	0.57	0.78	0.32	0.45	0.32	0.31	0.06	0.21	0.17	1.14	0.82	0.08	0.08
Total	*98.87*	98.04	95.40	94.69	98.40	98.93	96.10	98.71	97.39	97.38	96.12	97.11	98.55	98.10
	Mugearite solvent													
Sample	*Q*	Q1	Q1	Q2	Q2	Q3	Q3	Q4	Q4	Q7	Q7	Q8	Q8	Q6
Duration (min)		30	30	60	60	120	120	180	180	1440	1440	2880	2880	4320
Type	*Solvent*	B.L.	B.L.	BL	B.L.	B.L.	B.L.	B.L.	B.L.	B.L.	B.L.	B.L.	B.L.	B.L.
SiO_2	*54.01*	57.46	66.06	55.75	68.07	59.21	61.64	59.88	54.93	69.25	67.84	65.79	61.33	66.15
TiO_2	*3.46*	2.23	0.61	2.13	1.00	1.96	1.73	2.98	4.05	0.88	0.89	1.83	2.32	0.18
Al_2O_3	*11.47*	9.46	5.54	8.97	4.36	7.43	6.02	9.93	7.03	6.71	5.99	6.67	9.34	3.70
FeO	*7.33*	7.28	5.14	7.49	4.43	8.58	8.59	4.95	5.98	4.46	4.56	7.81	7.12	8.89
MnO	*0.16*	0.14	0.07	0.13	0.09	0.19	0.18	0.07	0.16	0.09	0.11	0.13	0.12	0.18
MgO	*6.77*	7.81	11.33	8.06	10.28	7.45	6.84	8.10	9.34	7.72	7.86	7.31	6.53	12.41
CaO	*8.36*	7.54	3.77	7.82	4.42	6.58	6.45	3.44	9.91	3.45	3.45	3.60	5.21	2.84
Na_2O	*5.56*	5.43	4.51	6.33	4.96	6.02	5.95	8.13	6.33	4.84	5.27	4.38	4.56	3.78
K_2O	*2.24*	2.14	2.46	1.62	2.21	1.89	1.98	2.29	1.40	2.51	2.40	1.93	2.04	1.77
P_2O_5	*0.63*	0.53	0.02	0.51	0.04	0.32	0.18	0.00	0.28	0.06	0.03	0.08	0.29	0.02
Total	*99.99*	100.00	99.52	98.79	99.85	99.65	99.56	99.78	99.40	99.97	98.40	99.53	98.86	99.92
	Phonotephrite solvent													
Sample	*DPX*	DPX-14	DPX-10	DPX-10	DPX-6	DPX-6	DPX-2	DPX-2	*DPX*	DPX-12	DXP-12	DPX-8	DPX-8	DPX-4
Duration (min)		244	860	860	1440	1440	2880	2880		860	860	1440	1440	2880
f_{O_2}	*Air*	Air	Air	Air	Air	Air	Air	Air	*QFM*	QFM	QFM	QFM	QFM	QFM
Type	*Solvent*	B.L.	B.L.	B.L.	B.L.	B.L.	B.L.	B.L.	*Solvent*	B.L.	B.L.	B.L.	B.L.	B.L.
SiO_2	*48.87*	62.39	65.41	63.55	55.86	56.11	66.94	67.35	*48.12*	63.39	65.78	62.29	61.10	65.55
TiO_2	*3.10*	0.71	2.44	4.22	1.94	1.98	0.21	0.23	*4.39*	1.48	1.69	2.54	4.41	0.12
Al_2O_3	*9.64*	8.07	4.57	4.40	9.94	10.12	4.42	4.55	*9.46*	4.28	4.41	7.01	6.96	3.70
FeO	*8.32*	7.80	6.12	6.27	8.34	8.78	6.38	6.61	*7.39*	3.74	4.18	4.26	4.16	4.03
MnO	*0.16*	0.13	0.07	0.15	0.16	0.21	0.08	0.09	*0.15*	0.15	0.11	0.15	0.06	0.11
MgO	*8.43*	5.75	8.73	8.59	8.05	7.48	8.98	8.69	*8.78*	11.20	10.79	10.12	9.72	11.80
CaO	*12.14*	4.00	3.66	3.80	8.36	7.48	4.12	4.20	*12.25*	7.04	4.99	5.28	5.22	4.56
Na_2O	*6.11*	5.52	6.62	6.56	5.06	4.58	6.11	5.96	*6.25*	6.73	6.72	6.50	6.33	8.13
K_2O	*2.45*	3.99	2.78	2.73	1.51	1.60	2.67	2.68	*2.46*	1.85	2.06	1.74	1.67	2.35
P_2O_5	*0.77*	0.00	0.00	0.00	0.66	0.76	0.01	0.02	*0.76*	0.05	0.04	0.30	0.35	0.02
Total	*99.99*	98.36	100.39	100.26	99.89	99.09	99.91	100.39	*100.01*	99.91	100.74	100.19	99.98	100.37

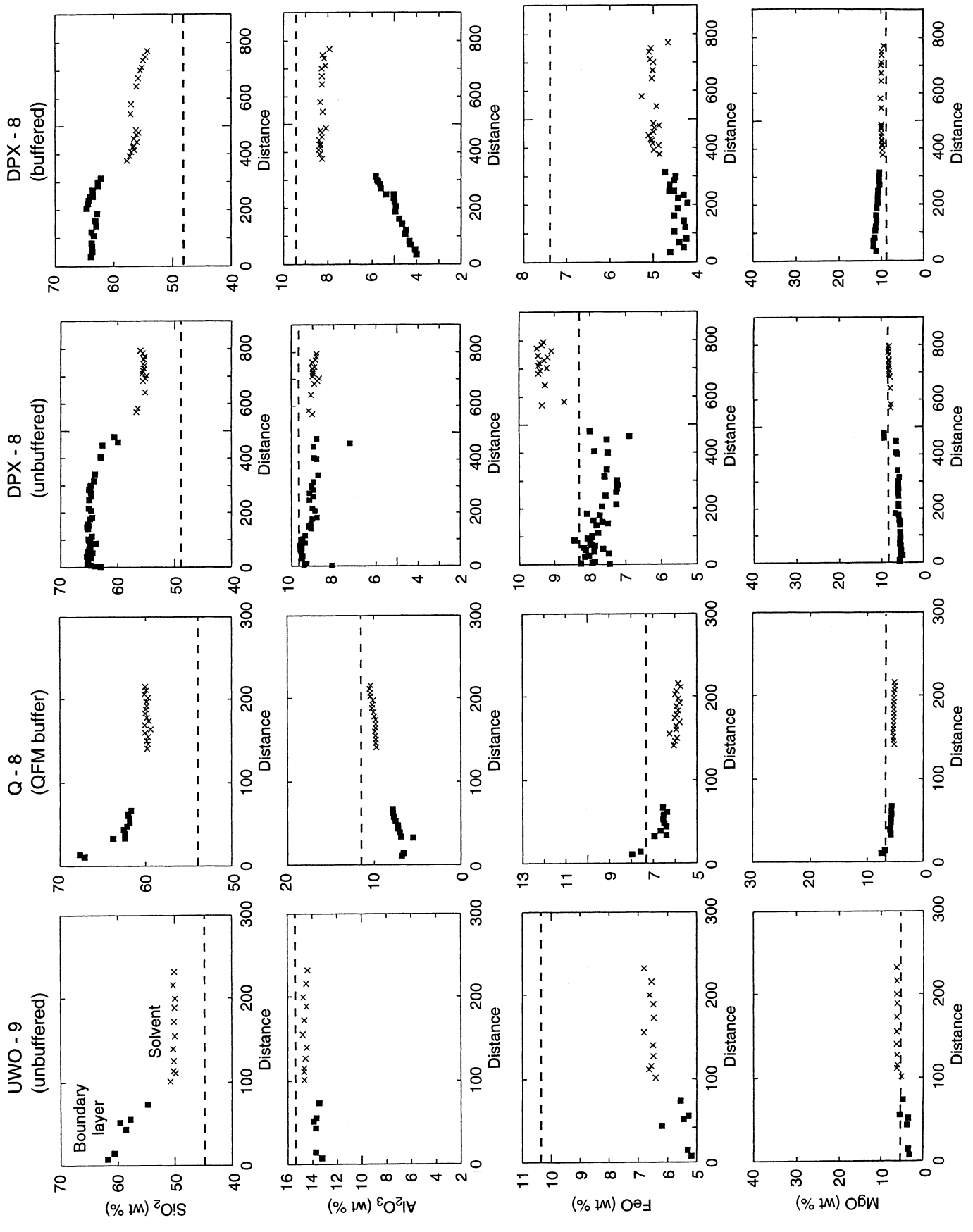
UWO - 9
(unbuffered)
Q - 8
(QFM buffer)
DPX - 8
(unbuffered)
DPX - 8
(buffered)
Boundary layer
Solvent
SiO2 (wt %)
Al2O3 (wt %)
FeO (wt %)
MgO (wt %)
Distance

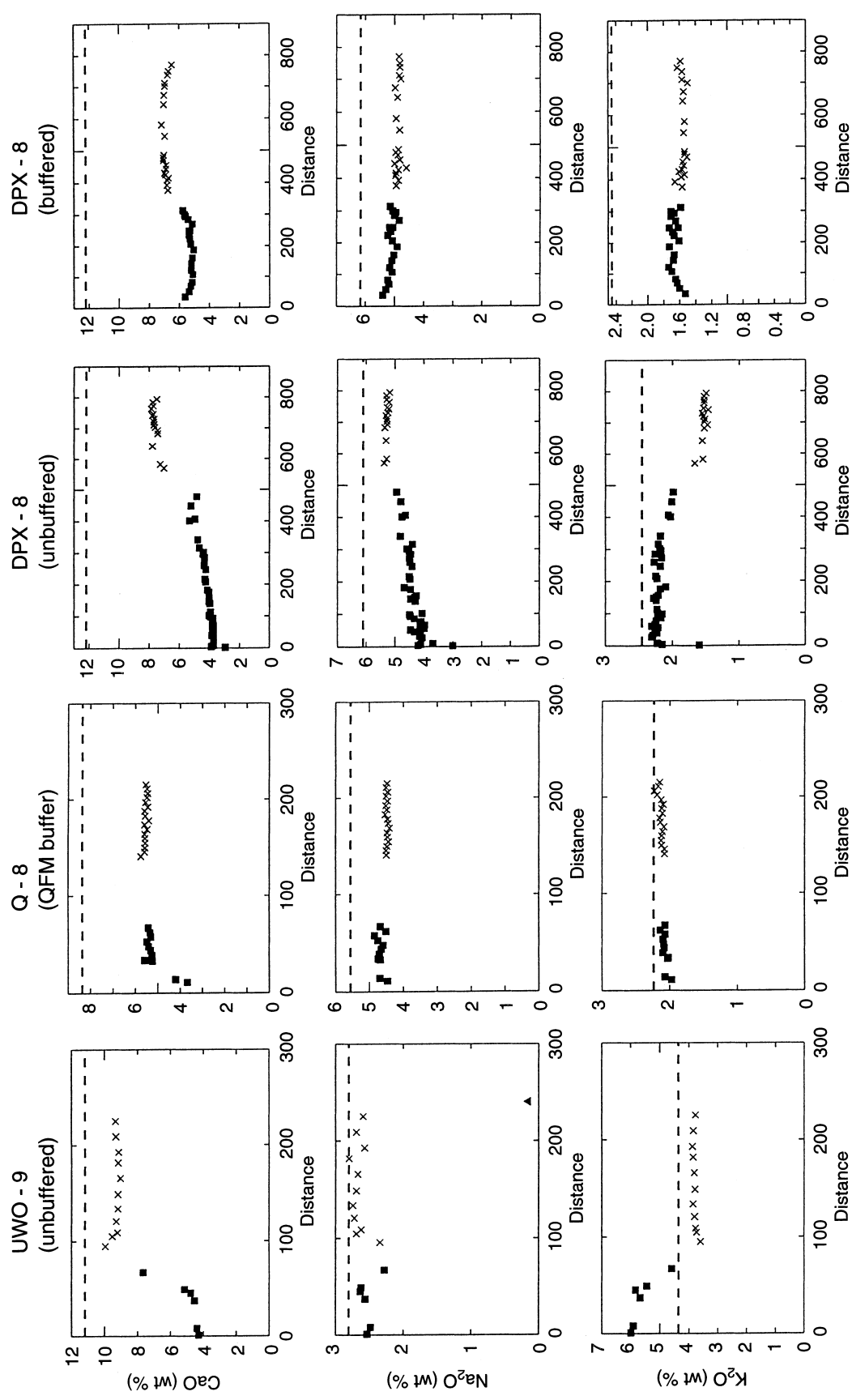

Fig. 4 Compositional profiles of glass from orthopyroxene (*on left of diagrams*) through the boundary layer (*solid squares*) to the solvent (*crosses*). The *dashed line* marks the original composition of the solvent before dissolution of orthopyroxene

buffered experiments the K_2O concentration is approximately equal to the solvent.

These results suggest that the differences between the mugearite and basanite experiments described in the earlier sections are due more to the difference in f_{O_2} rather than to compositional effects. We explore the reason for this in a later section.

Comparison of experiments with nature

Compositions of glass in a naturally dissolved orthopyroxene from Gees, West Eifel, Germany, are shown in Fig. 5. In this example, glass in the boundary layer adjacent to the solvent melt is strongly enriched in SiO_2 and K_2O relative to the solvent and depleted in FeO and CaO. Al_2O_3 and Na_2O do not have coherent patterns. The best comparison between the experimentally determined profiles and the natural example are for the experiments conducted in air. In all cases these show enrichment in both SiO_2 and K_2O relative to the solvent. In contrast the buffered experiments do not show any distinctive K_2O enrichment. This comparison suggests that in the natural examples given here the reaction between Si-undersaturated melt and orthopyroxene took place under relatively oxidising conditions.

Solvent glass adjacent to boundary layers

In the three series of experiments glass in the solvent surrounding the boundary layer is distinct in composition from the starting solvent (Fig. 4) and shows similar trends of enrichment to the glass in the boundary layer. However, the solvents are not as enriched in SiO_2 as the boundary layer (Fig. 4, Table 6). Since the solvent acts as a source for elements diffusing into the boundary

Fig. 5 Compositional traverse across a reacted orthopyroxene crystal in a mantle xenolith from Gees, West Eifel, Germany (see Fig. 2f)

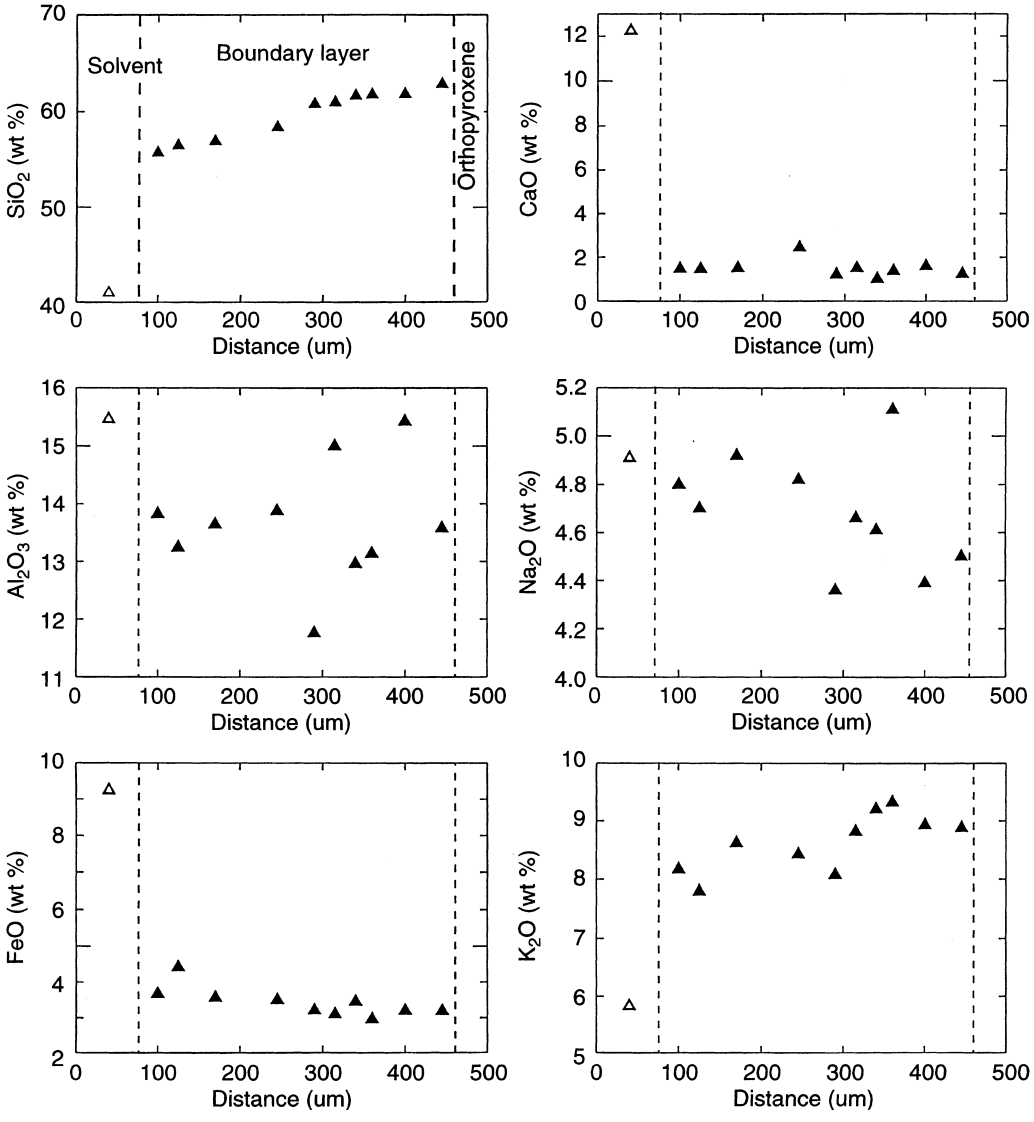

Table 6 Composition of solvent melts after dissolution experiments

	Basanite					Mugearite					Phonotephrite			Phonotephrite		
Sample	*UWO*	UWO-2	UWO-5	UW0-9	UW0-12	*Q*	Q1	Q3	Q4	Q8	*DPX*	DPX-6	DPX-2	*DPX*	DPX-8	DPX-4
Duration (min)		30	180	720	2880		30	120	180	2880		1440	2880		1440	2880
f_{O_2}	*Original*	Solvent	Solvent	Solvent	Solvent	*Original*	Solvent	Solvent	Solvent	Solvent	*Original*	Air	Air	*QFM*	QFM	QFM
Type	*Solvent*					*Solvent*					*Solvent*	Solvent	Solvent	*Original Solvent*	Solvent	Solvent
SiO_2	*45.49*	47.37	49.00	50.30	49.19	*54.01*	54.55	55.49	55.04	56.92	48.87	54.64	53.02	*48.12*	60.65	56.03
TiO_2	*3.06*	2.78	2.54	3.00	2.84	*3.46*	2.38	2.50	4.06	2.73	3.10	1.74	2.04	*4.39*	2.57	1.57
Al_2O_3	*15.98*	13.63	11.13	14.50	12.82	*11.47*	9.78	9.14	7.04	12.49	9.64	9.75	9.12	*9.46*	7.78	7.54
FeO	*10.17*	9.45	8.54	6.55	8.31	*7.33*	7.78	8.14	5.99	6.95	8.32	8.91	7.67	*7.39*	4.78	5.33
MnO	*0.16*	0.17	0.22	0.18	0.23	*0.16*	0.08	0.13	0.16	0.15	0.16	0.11	0.20	*0.15*	0.13	0.10
MgO	*5.06*	7.47	9.97	6.33	7.66	*6.77*	8.07	7.51	9.36	6.12	8.43	8.25	8.27	*8.78*	9.69	11.49
CaO	*11.85*	9.81	12.28	9.32	10.74	*8.36*	8.86	8.22	9.93	6.75	12.14	8.76	10.32	*12.25*	5.90	8.22
Na_2O	*2.53*	2.32	1.69	2.69	2.13	*5.56*	6.15	6.08	6.34	4.90	6.11	5.04	6.59	*6.25*	6.76	6.68
K_2O	*3.90*	3.74	2.72	3.86	3.30	*2.24*	1.71	1.76	1.40	1.82	2.45	1.49	1.99	*2.46*	1.73	1.79
P_2O_5	*0.67*	0.63	0.51	0.71	0.63	*0.63*	0.53	0.58	0.28	0.46	0.77	0.76	0.56	*0.76*	0.40	0.50
Total	*98.87*	98.37	98.60	97.44	97.85	*99.99*	99.89	99.55	99.59	99.30	99.99	99.45	99.78	*100.01*	100.38	99.25

layer it should be progressively depleted in Al, Fe, Ca, Na and K as these elements move into the boundary layer. This depletion is present but is not as large as expected. This with the approximately constant thickness of the boundary layers suggests that the boundary layer and solvent mixed over the duration of the experiment. The lack of compositions approaching the original solvent, even in experiments of very short duration, suggests that the mixing was not due to diffusion but more likely was a bulk mixing process. This is further supported by the distinct compositional discontinuities at the solvent – boundary layer interface. In the case where diffusion was dominant we would expect a smooth transition across this interface and a gradual tailing off of compositions toward the original solvent composition.

Boundary layer olivine

Olivine in the boundary layers is MgO-rich with Fo contents of 0.87 to 0.98 (Table 7). There is no systematic difference in composition between the different solvent compositions. However, olivine from the oxidised phonotephrite experiments has higher Mg# Mg/(Mg + Fe) than that from the experiments equilibrated at the QFM buffer since Fe_2O_3 is excluded from olivine. Calculated partition coefficients (using all Fe as FeO) for Mg and Fe between olivine and the surrounding melt range from 0.1 to 0.3. The lowest values are those from olivine – melt pairs where the glass is strongly enriched in SiO_2 and alkalis. The less siliceous glasses have K_ds closer to the equilibrium value of 0.3 (Roeder and Emslie 1970). However, in our experiments since a significant proportion of the Fe in the melt is present as Fe^{3+} the calculated K_d values will be artificially low. An alternative explanation for low K_d values has been proposed by Draper and Green (1997) to explain why Fe-Mg K_d values for olivine – Si-rich liquid pairs in their experiments are consistently lower than the equilibrium value for mafic melts. They suggest that these values represent

Table 7 Olivine compositions from reaction zones

	Basanite	Mugearite		Phonotephrite	
Sample	UWO-8	Q2	Q8	DPX-2	DPX-4
Duration	1260	60	2880	2880	2880
f_{O_2}	Air	QFM	QFM	Air	AFM
SiO_2	41.87	42.56	41.25	44.28	42.69
Ti_2O	0.06	0.05	0.00	0.00	0.00
Al_2O_3	0.06	0.01	0.05	0.01	0.02
FeO	5.68	5.01	13.09	1.45	5.34
MnO	0.23	0.12	0.19	0.12	0.12
MgO	51.94	51.27	45.61	54.70	52.47
CaO	0.29	0.33	0.41	0.23	0.27
Na_2O	0.00	0.08	0.01	0.07	0.06
K_2O	0.02	0.02	0.01	0.01	0.00
Total	100.15	99.45	100.62	100.86	100.86
Mg#	0.95	0.95	0.87	0.98	0.95

true equilibrium partititioning for highly evolved Si-alkali-rich melts. Thus, in our experiments the low K_d values in the Si-rich melts may not be evidence of disequilibrium.

The presence of 20 to 30% olivine in the reaction zones cannot be attributed simply to incongruent dissolution of orthopyroxene since Bowen & Andersen (1914) showed that the percentage olivine produced on incongruent melting of olivine was approximately 5 to 6%. We suggest then, that a small amount of the olivine in the reaction zone formed by incongruent dissolution of orthopyroxene but that the majority formed due to changes in the phase relations of the solvent on mixing with the liquid derived from orthopyroxene breakdown.

Boundary layer clinopyroxene

Clinopyroxene in the boundary layer is SiO_2 and MgO-rich and FeO and CaO-poor relative to that in the original solvent (Tables 8, 4). Within the three groups of experiments there are minor differences in the Na content of the clinopyroxene that appear to reflect differences in the original solvent composition. In common with olivine, the experiments using a phonotephrite solvent show a distinct difference in pyroxene Mg# depending on the f_{O_2} at which the experiment was equilibrated. In the oxidised experiments the clinopyroxene has lower Mg# than in the more reduced runs suggesting that those in the oxidised experiments contain a significant amount of Fe_2O_3. Clinopyroxene – liquid equilibria calculations (Nielsen and Drake 1979) gave K_d values of 0.13 to 0.39 with most being in the range 0.25 to 0.31, indicating that most clinopyroxenes are in equilibrium with the surrounding melt. Clinopyroxenes that give low K_d values commonly have a hopper texture that suggests that they may have formed on quenching of the samples. A similar problem exists in the calculation of K_d values for clinopyroxene as described for olivine, i.e. a high proportion of Fe^{3+} in the melt may result in low calculated K_ds when the calculations are made using all iron as FeO.

Discussion

Comparison of experimental and natural Si-rich glass

Figure 3 shows a comparison of the experimentally produced Si-rich glass with the two fields defined for orthopyroxene-rich and orthopyroxene-poor glasses. With the exception of Al_2O_3 the solvent melts fall within or close to the field defined for glass in orthopyroxene-rich xenoliths. The boundary layer glass shows similar compositional trends to natural glass in orthopyroxene-rich xenoliths. Again with the exception of Al_2O_3, the overall concentration of each oxide is well within the range of natural glass compositions. The low Al_2O_3 contents of the boundary layer glasses likely reflect the low Al_2O_3 in the starting solvent. However, we cannot rule out the possibility that an aluminous phase such as spinel was involved in the reaction in nature.

It has been suggested that xenolith glasses can form by a wide variety of processes (Table 1). Nevertheless, the distinct compositional grouping with respect to the host orthopyroxene content coupled with the results of the present study suggest that dissolution of orthopyroxene plays a significant role in glass formation. Previous studies have suggested that Si-rich glass may have formed in the mantle prior to xenolith entrainment. At pressures greater than approximately 5 kbar the breakdown of orthopyroxene is no longer incongruent. Thus, at high pressure extreme silica enrichment is unlikely since the reaction will involve simple mixing of orthopyroxene and solvent.

Our results suggest that it is likely that at least some Si-rich xenolith glass formed at low pressure, possibly by reaction between orthopyroxene and infiltrated host magma, which in almost all cases is Si-undersaturated. A detailed investigation of the effects of pressure on orthopyroxene dissolution is currently underway.

Table 8 Composition of clinopyroxene in reaction zones

	Basanite			Mugearite		Phonotephrite			
Sample	UWO-2	UWO-5	UWO-9	Q-3	Q8	DPX-6	DPX-8	DPX-14	DPX-16
Duration	30	180	720	120	2880	1440	1440	244	244
fo_2	Air	Air	Air	QFM	QFM	Air	QFM	Air	QFM
SiO_2	49.11	55.80	51.36	55.66	56.73	55.30	55.05	54.86	55.90
TiO_2	1.08	0.20	0.56	1.48	0.34	0.26	3.31	1.60	1.76
Al_2O_3	3.69	0.50	2.43	5.28	2.67	0.75	0.21	1.79	0.25
FeO	5.74	2.63	5.25	4.84	5.42	3.92	2.00	4.38	2.63
MnO	0.13	0.16	0.12	0.12	0.13	0.10	0.00	0.00	0.00
MgO	17.29	26.09	18.94	12.79	18.63	17.58	19.38	17.17	21.30
CaO	21.27	14.21	20.26	14.71	14.66	21.00	19.45	17.39	16.63
Na_2O	0.41	0.84	0.78	3.37	1.56	1.00	1.05	1.80	0.77
K_2O	0.07	0.02	0.00	0.88	0.46	0.00	0.00	0.06	0.05
Total	98.79	100.45	99.70	99.14	100.59	99.91	100.44	99.05	99.30
Mg#	0.85	0.95	0.88	0.84	0.87	0.90	0.95	0.88	0.94

Mechanism of dissolution

The reactions observed in the experiments are due to disequilibrium between a melt with low silica activity and orthopyroxene. Since the orthopyroxene crystal does not break down to a melt of its own composition, the process can be termed incongruent dissolution (Oishi et al. 1965). In this process a solid is converted by dissolution to a liquid and another solid both of different composition from the original solid and melt. In the system Fo + SiO_2 enstatite breaks down at 1559 °C at 1 atmosphere to form forsterite + silica (Bowen and Anderson 1914). In a multicomponent system, this breakdown occurs at much lower temperature (cf. Fisk 1986). In a natural system where the orthopyroxene contains small amounts of Al_2O_3, CaO and Na_2O these components will be released to the melt resulting in a silica-rich melt with small amounts of Al etc. Assuming that the experimental data for incongruent melting of pure enstatite Bowen & Andersen (1914) can be extrapolated to our experiments the amount of olivine that should be formed on incongruent melting is approximately 6%. However, in all of our experiments and in the natural examples of dissolved orthopyroxene the proportion of olivine is much higher. This requires an additional oliving forming process. We suggest that the additional olivine crystallised due to progressive changes in the phase relations of the solvent as it mixes with liquid derived from orthopyroxene breakdown.

Clinopyroxene is not a normal product of the incongruent breakdown of orthopyroxene either in simple systems or during reaction with basalt (Fisk 1986). However, it is commonly associated with reaction zones between orthopyroxene and melt in nature (Wilshire and Binns 1961; Tracy 1980; Kuo and Essene 1986; Shaw and Edgar 1997). The components required for clinopyroxene formation must have diffused into the boundary layer from the solvent. This is clear from the zoned nature of the boundary layer in the short duration experiments where clinopyroxene is concentrated in the outer regions, i.e. where clinopyroxene saturation would occur first.

An alternative explanation is that dissolution of orthopyroxene in a melt where clinopyroxene is the liquidus phase is likely to result in crystallisation of clinopyroxene, i.e. the phase in which the solvent is saturated (Bowen 1922).

Diffusion into the boundary layer

SiO_2 enrichment decreases outward from the boundary layer to the solvent showing that Si diffused down its concentration gradient toward the Si-poor solvent. In the reduced experiments Al_2O_3 also diffused down its concentration gradient toward the Al-poor boundary layer melt but at a slower rate than in the oxidised experiments where the flat profile is evidence of rapid diffusion. To a lesser extent the same is true for CaO.

The concentrations of FeO and MgO are buffered by olivine and clinopyroxene crystallisation and in general these profiles are flat suggesting rapid diffusion and equilibration of the ions in the two melts. The relatively flat profiles for Na_2O also indicate rapid diffusion and attainment of equilibrium between solvent and boundary layer. In the reduced f_{O_2} experiments with the phonotephrite solvent the increased concentrations in the most Si-rich part of the boundary layer suggest that Na may have diffused against its concentration gradient. We explore this phenomenon further below.

In reduced f_{O_2} experiments K and Na show similar behaviour between the solvent and boundary layer melts. However, under oxidising conditions K_2O concentrations are higher in the Si-Al-rich melt in the boundary layer than in the solvent suggesting that K_2O was able to diffuse uphill i.e. against its own concentration gradient. This type of behaviour has been attributed to the strong preference of K and Na for polymerised Si and Al-rich melts over depolymerised Si- and Al-poor ones (Ryerson and Hess 1978; Watson 1982). The difference between the profiles in the oxidised and reduced experiments appears to be due to the concentration of Al, a network forming cation. Since Al abundance is lower under reduced conditions the boundary layer melt was less polymerised and was therefore less likely to accommodate uphill diffusion of K and Na.

The inward diffusion of components towards the orthopyroxene will require a flux of charge balancing species in the opposite direction. Figure 4 shows that the dominant flux of material outwards is of Si. In this case Si must be the charge balancing cation. This seems reasonable since to account for the divalent cations only half as much Si must diffuse out to compensate for charge and for the alkalis only a quarter as much Si must diffuse out. This observation suggests that the diffusivity of Si plays a major role in controlling the mobility of the faster diffusing cations as has also been noted by Harrison and Watson (1983).

The distinct differences in the concentration profiles between the buffered and unbuffered experiments (phonotephrite experiments) indicates that f_{O_2} plays a major role in influencing the composition of glass formed during orthopyroxene dissolution. The main differences between the buffered and unbuffered experiments are in Al, Na and K as well as in the overall abundance of iron (as measured by microprobe). Clearly, the experiments equilibrated in air will contain considerably more Fe^{3+} than Fe^{2+} which is likely to have an effect on the structure of the melt. In the buffered samples where the Fe^{2+}/Fe^{3+} ratio is high Al diffusion into the boundary layer glass was slow compared to the more oxidised experiments. This may be due to the changing role of iron from reduced to oxidised conditions. Ferrous iron is generally considered to act as a network modifier whereas ferric iron can act both as a network modifier and a network former (Mysen 1986). It is not clear if the differences in the

profiles are due to charge balance considerations or if they reflect real changes in the structure of the melt. Further experiments to investigate this are in progress.

Convective mixing between boundary layer and solvent

The contamination of the solvent outside the boundary layer is achieved by mixing of the boundary layer melt with the solvent. Examination of the boundary layer thickness and chemical profiles suggests that this mixing is not due to diffusion alone, but more likely to convective mixing brought on by density and viscosity contrasts between the two melts that caused a hydrodynamic instability that in turn led to the onset of convection (Cooper and Kingery 1964; Donaldson 1993; McLeod et al. 1996). Donaldson (1990) notes that the density difference required to cause convection is approximately 2% of the density of the bulk melt. Calculated density differences between solvent and the melt at the edge of the boundary layers give a contrast of 15, 5 and 7% for the basanite, mugearite and phonotephrite experiments respectively. However, it must be noted that the density contrasts will be reduced as convection occurs and contaminates the solvent melt with silica. Besides density induced convection, the movement of small trapped gas bubbles may induce forced convection (Donaldson 1990). Though convection appears to have been active during orthopyroxene dissolution, it did not reach the crystal itself since compositional gradients and the boundary layer are still preserved.

Convergence of boundary layer melt compositions

Francis (1987) suggested that the composition of basaltic melts buffered by lherzolite would be broadly andesitic at 1 bar. In this study we show that while this assertion is broadly correct, it is possible to produced much more siliceous melts, particularly at the orthopyroxene – solvent interface. In general, despite the widely varying starting compositions used the melts all show similar compositional trends and in fact in most cases the boundary layer melt compositions converge at high silica contents giving melts of trachyandesitic, trachytic and rhyolitic compositions.

Conclusions

(1) Low pressure reaction of orthopyroxene with Si-undersaturated alkaline melts results in incongruent dissolution of orthopyroxene to form olivine and a Si-rich melt. Further crystallisation of olivine from the hybrid boundary layer melt results in considerable Si-enrichment.
(2) Diffusion of components from the solvent to the boundary layer results in enrichment of the boundary layer in Ca, Al, Na and K. The Ca-enrichment results in clinopyroxene crystallisation. Diffusion is mainly down the concentration gradient except for alkalis which show a marked preference for the Si-rich melts. Charge balance during diffusion is maintained by outward diffusion of silica. The f_{O_2} at which dissolution occurs plays a major role in determining the diffusivity of ions particularly Al, K and Na.
(3) The solvent surrounding the boundary layer is contaminated with boundary layer components as a result of convective mixing brought on by density contrasts between the two melts.
(4) The Si-rich melts formed by orthopyroxene dissolution are very similar to extreme composition glasses commonly found in mantle xenoliths. The xenolith glasses are commonly thought to have formed in situ in the mantle prior to transport to surface. This work suggests that at least some Si- and alkali-rich xenolith glasses may have formed by host magma – orthopyroxene reaction at low pressure.
(5) The dissolution process cannot be modelled successfully unless the original solvent composition is known.

Acknowledgements We thank John Forth and Gord Wood (UWO) and Hubert Schulze (BGI) for preparing the polished sections. Thanks also to Don Dingwell for his assistance in setting up the gas mixing furnaces and the f_{O_2} sensors. Reviews from B. Tracy, C. Szabo and B Watson improved an earlier version of this paper. ADE gratefully acknowledges funding from NSERC (Canada).

References

Albee AL, Ray L (1970) Correction factors for the electron microanalysis of silicates, oxides, carbonates, and sulphates. Anal Chem 42: 1408

Bailey DK (1987) Mantle metasomatism – perspective and prospect, In: Fitton JG, Upton BGJ (eds) Alkaline igneous rocks. Geol Soc London Spec Pub 30: 1–13

Bottinga Y, Weill DF (1970) Densities of liquid silicate systems calculated from partial molar volumes of oxide components. Am J Sci 269: 169–182

Bottinga Y, Weill DF, Richet P (1982) Density calculations dor silicate liquids – 1. Revised method for aluminosilicate compositions. Geochim Cosmochim Acta 46: 909–919

Bowen NL (1922) The behaviour of inclusions in igneous magmas. J Geol 30: 513–570

Bowen NL, Anderson O (1914) The binary system MgO – SiO_2. Am J Sci 37: 487–500

Boyd FR, England JL, Davis BTC (1964) Effects of pressure on the melting and polymorphism of enstatite, $MgSiO_3$. J Geophys Res 69: 2101–2109

Brearly M, Scarfe CM (1986) Dissolution rates of upper mantle minerals in an alkali basalt melt at high pressure: an experimental study and implications for ultramafic xenolith survival. J Petrol 27: 1157–1182

Carpenter RL (1996) Petrology of mantle xenoliths hosted in Tertiary magmas of the Hessian Depression, Germany: a comparison to xenoliths From Quaternary magmas of the West Eifel. MSc thesis, University of Western Ontario, London, Ontario, Canada

Chazot G, Menzies M, Harte B (1996) Silicate glasses in spinel lherzolites from Yemen: origin and chemical composition. Chem Geol 134: 159–179

Cooper AR, Kingery WD (1964) Dissolution in ceramic Systems: I. Molecular diffusion, natural convection, and forced convection studies of sapphire dissolution in calcium aluminum silicate. J Am Ceram Soc 47: 37–43

Dautria JM, Dupuy C, Takherist D, Dostal J (1992) Carbonate metasomatism in the lithospheric mantle: peridotitic xenoliths from a melilititic district of the Sahara basin. Contrib Mineral Petrol 111: 37–52

Donaldson CH (1990) Forsterite dissolution in superheated basaltic, andesitic and rhyolitic melts. Mineral Mag 54: 67–74

Donaldson CH (1993) Convective fractionation during magnetite and hematite dissolution in silicate melts. Mineral Mag 57: 469–488

Draper DS (1992) Spinel lherzolite xenoliths from Lorena Butte, Simcoe Mountains, Southern Washington (USA). J Geol 100: 766–776

Draper DS, Green TH (1997) P-T phase relations of silicic, alkaline, aluminous mantle -xenolith glasses under anhydrous and C-O-H fluid-saturated conditions. J Petrol 38: 1187–1224

Edgar AD (1997) Mantle metasomatism: constraints and cautions, In: Gupta AK, Onuma K, Arima M (eds) Synthetic and natural rock systems (Kenzo Yagi Volume). Allied Publishers, Bangalore, India pp 182–195

Edgar AD, Lloyd FE, Forsyth DM, Barnett RL (1989) Origin of glass in upper mantle xenoliths from the quaternary volcanics of Gees, West Eifel, Germany. Contrib Mineral Petrol 103: 277–286

Edwards BR, Russell JK (1996) A review and analysis of silicate mineral dissolution experiments in natural silicate melts. Chem Geol 130: 233–245

Fisk MR (1986) Basalt magma interaction with harzburgites and the formation of high-magnesium andesites. Geophys Res Lett 13: 467–470

Francis DM (1976a) Amphibole pyroxenite xenoliths: cumulate or replacement phenomena from the upper mantle, Nunivak Island, Alaska. Contrib Mineral Petrol 58: 51–61

Francis DM (1976b) The origin of amphibole in lherzolite xenoliths from Nunivak Island, Alaska. J Petrol 17: 357–378

Francis D (1987) Mantle-melt interaction recorded in spinel lherzolite xenoliths from the Alligator Lake Volcanic Complex, Yukon, Canada. J Petrol 28: 569–597

Frey FA, Green DH (1974) The mineralogy, geochemistry and origin of lherzolite inclusions in Victoria basanites. Geochim Cosmochim Acta 38: 1023–1059

Gamble JA, Kyle PR (1987) The origins of glass and amphibole in spinel-wehrlite xenoliths from Foster Crater, McMurdo Volcanic Group, Antarctica. J Petrol 25: 755–779

Garcia MO, Presti AA (1987) Glass in garnet pyroxenite xenoliths from Kaula Island, Hawaii: product of infiltration of host nephelinite. Geology 15: 904–906

Ghiorso MS, Sack RO (1995) Chemical mass transfer in magmatic processes. IV. A revised and internally consistent thermodynamic model for the interpolation and extrapolation of liquid – solid equilibria in magmatic systems at elevated temperatures and pressures. Contrib Mineral Petrol 119: 197–212

Hansteen TH, Andersen T, Neumann E-R, Jelsma H (1991) Fluid and silicate glass inclusions in ultramafic and mafic xenoliths from Hierro, Canary Islands: implications for mantle metasomatism. Contrib Mineral Petrol 107: 242–254

Harrison TM, Watson EB (1983) Kinetics of zircon dissolution and zirconium diffusion in granitic melts of variable water content. Contrib Mineral Petrol 84: 66–72

Hauri EH, Shimizu N, Dieu JJ, Hart SR (1993) Evidence for hotspot-related carbonatite metasomatism in the oceanic upper mantle. Nature 365: 221–227

Hermes OP, Cornell WC (1981) Quenched crystal mush and associated magma compositions as indicated by intercumulus glasses from Mt. Vesuvius. J Volcanol Geotherm Res 9: 133–149

Ionov DA, Dupuy C, O'Reilly SY, Kopylova MG, Genshaft YS (1993) Carbonated peridotite xenoliths from Spitzbergen: implications for trace element signature of mantle carbonate metasomatism. Earth Planet Sci Lett 119: 283–297

Ionov DA, Hofmann AW, Shimizu N (1994) Metasomatism-induced melting in mantle xenoliths from Mongolia. J Petrol 35: 753–785

Jones AP, Smith JV, Dawson JB (1983) Glasses in mantle xenoliths from Olmani, Tanzania. J Geol 91: 167–178

Kuo LC, Essene EJ (1986) Petrology of spinel harzburgite xenoliths from the Kishb Plateau, Saudi Arabia. Contrib Mineral Petrol 93: 335–346

Kuo L-C, Kirkpatrick RJ (1985) Kinetics of crystal dissolution in the system diopside-forsterite-silica. Am J Sci 285: 51–90

McLeod P, Riley DS, Sparks RSJ (1996) Melting of a sphere in hot fluid. J Fluid Mech 327: 393–409

Menzies M, Rogers N, Tindle A, Hawkesworth C (1987) Metasomatic and enrichment processes in lithospheric peridotites, an effect of asthenosphere-lithosphere interaction. In: Menzies MA, Hawkesworth CJ (eds) Mantle metasomatism. Academic Press, London pp 313–361

Mysen BO (1986) Structure and petrologically important properties of silicate melts relevant to natural magmatic liquids. In: Scarfe CM (ed) Short course in silicate melts. Mineralogical Association of Canada, Nepean, Ontario pp 180–235

Nielsen CH, Sigurdsson H (1981) Quantitative methods for electron microprobe analysis of sodium in natural and synthetic glasses. Am Mineral 66: 547–552

Nielsen RL, Drake MJ (1979) Pyroxene-melt equilibria. Geochim Cosmochim Acta 43: 1259–1272

O'Connor TK, Edgar AD, Lloyd FE (1996) Origin of glass in Quaternary mantle xenoliths from Meerfeldermaar, West Eifel, Germany: implications for enrichment in the lithospheric mantle. Can Mineral 34: 187–200

Oishi Y, Cooper AR, Kingery WD (1965) Dissolution in ceramic systems: III. Boundary layer concentration gradients. J Am Ceram Soc 48: 88–95

Padovani ER, Carter JL (1977) Aspects of deep crustal evolution beneath south central New Mexico. Geophys Monogr Am Geophys Union 20: 19–55

Roeder PL, Emslie RF (1970) Olivine liquid equilibrium. Contrib Mineral Petrol 29: 275–289

Ryerson FJ, Hess PC (1978) Implication of liquid-liquid distribution coefficients to mineral – liquid partitioning. Geochim Cosmochim Acta 42: 921–932

Schiano P, Clocchiatti R (1994) Worldwide occurrence of silica-rich melts in sub-continental and sub-oceanic mantle minerals. Nature 368: 621–624

Schiano P, Clocchiatti R, Shimizu N, Weis D, Mattielli N (1994) Cogenetic silica-rich and carbonate-rich melts trapped in mantle minerals in Kerguelen ultramafic xenoliths: Implications for metasomatism in the oceanic upper mantle. Earth Planet Sci Lett 123: 167–178

Shaw CSJ, Edgar AD (1997) Post-entrainment mineral-melt reactions in spinel peridotite xenoliths from Inver, Donegal, Ireland. Geol Mag 134: 771–779

Szabo C, Bodnar RJ, Sobolev AV (1996) Metasomatism associated with subduction-related, volatile-rich silicate melt in the upper mantle beneath the Nograd-Gomor Volcanic Field, Northern Hungary/Southern Slovakia: evidence from silicate melt inclusions. Eur J Mineral 8: 881–899

Thornber CR, Huebner JS (1985) Dissolution o olivine in basaltic liquids: experimental observations and applications. Am Mineral 70: 934–945

Tracy RJ (1980) Petrology and significance of an ultramafic xenolith suite from Tahiti. Earth Planet Sci Lett 48: 80–96

Watson EB (1982) Basalt contamination by continental crust: some experiments and models. Contrib Mineral Petrol 80: 73–87

Wilshire HG, Binns RA (1961) Basic and ultrabasic xenoliths from volcanic rocks of new South Wales. J Petrol 2: 185–208

Wilshire HG, McGuire AV (1996) Magmatic infiltration and melting in the lower crust and upper mantle beneath the Cima volcanic field, California. Contrib Mineral Petrol 123: 135–374

Yaxley GM, Kemenetsky V, Green DH, Falloon TJ (1997) Glasses in mantle xenoliths from western Victoria, Australia, and their relevance to mantle processes. Earth Planet Sci Lett 148: 433–446

Zinngrebe E, Foley SF (1995) Metasomatism in mantle xenoliths from Gees, West Eifel, Germany: evidence of calc-alkaline glasses and metasomatic Ca-enrichment. Contrib Mineral Petrol 122: 79–96